Semiclassical approaches to below-threshold harmonics

James A. Hostetter,[1] Jennifer L. Tate,[1] Kenneth J. Schafer,[1,2] and Mette B. Gaarde[1,2]
[1]*Department of Physics and Astronomy, Louisiana State University, Baton Rouge, Louisiana 70803-4001, USA*
[2]*PULSE Institute, SLAC National Accelerator Laboratory, Menlo Park, California 94025, USA*
(Received 4 May 2010; published 2 August 2010)

We study the generation of below-threshold harmonics in a model atom by extending the three-step semiclassical model of harmonic generation to include effects of the atomic potential. We explore the generalization of semiclassical trajectories of the electron in the presence of the combined laser-atom potential and calculate the intensity-dependent dipole phase associated with these trajectories. Our results are in good agreement with fully quantum mechanical calculations, as well as with recent experimental observations. We show that the so-called long trajectory readily generalizes to below-threshold harmonic generation and is relatively insensitive to the choice of initial conditions. We also find that the short trajectory can only lead to low-energy harmonics for electrons that have been released close to the ion core in a process that is closer to multiphoton than to tunnel ionization.

DOI: 10.1103/PhysRevA.82.023401 PACS number(s): 32.80.Rm, 42.65.Ky, 32.80.Wr

I. INTRODUCTION

In a recent experimental and theoretical study, Yost and collaborators investigated the generation of relatively low-order harmonics in xenon by an intense, 1.07-μm infrared laser field [1]. These harmonics, with photon energies below and close to the ionization threshold in xenon, were found to exhibit pronounced characteristics of semiclassical contributions to their generation process. In particular, interference between contributions with different intensity-dependent phases was observed in the yield of harmonics as low as the seventh, and the spectral and spatial profiles of these harmonics exhibited clear signatures of a contribution with a large, intensity-dependent phase. This earlier study discussed that these results can be understood in a generalized semiclassical model (SCM) of harmonic generation in which the atomic potential is included [1]. In the present article we discuss this generalized model in detail and elaborate on how some elements of low-order harmonic generation can be understood in terms of semiclassical dynamics.

The generation of harmonics with energies much higher than the ionization potential is well understood using the standard SCM [2–4]. In this model harmonics are produced in three steps: (i) An electron tunnel ionizes due to the laser field, (ii) is accelerated by the laser field far away from the parent atom, and (iii) may return to the parent atom when the laser field changes direction, where it can recombine and thereby release a photon with energy $E_{\rm ph} = T_r + I_p$. Here T_r is the kinetic energy gained from the field and I_p is the ionization potential of the atom. This model predicts not only the observed high harmonic cutoff (given by the maximum value of $T_r + I_p = 3.2U_p + I_p$, where the ponderomotive energy U_p is the cycle-averaged kinetic energy of the electron in the field) but also explains the intensity-dependent phase behavior of the emitted harmonics in terms of classical trajectories for tunnel-ionized electrons [5–7]. For each return energy below the cutoff energy, two electron trajectories with travel times of less than one optical cycle are found: the long trajectory which ionizes early and returns after a long travel time and the short trajectory which ionizes later and returns quickly. The phase acquired by the electron wave function along each trajectory, given by the action integral, is proportional to the cycle-averaged intensity and is in general very different for the short and long trajectories [6,8–11]. This gives rise to interference effects as a function of laser intensity, such as observed in [1,12,13].

In the standard SCM the effect of the atomic potential is ignored in the second step and the lowest possible value of T_r is zero, so by definition it cannot describe the generation of harmonics with energies $E_{\rm ph} < I_p$. In this article, we study the generation of below- and around-threshold harmonics in a generalized SCM which includes the atomic potential in both the initial ionization process and the subsequent continuum dynamics. Our approach is similar in spirit to that of [14–16], in which the classical dynamics of an electron in a combined laser-atom potential was invoked to explore strong-field single or double ionization. We find that there are classical trajectories that lead to electrons returning with below-threshold total energies and that the long trajectory in particular can be readily generalized to below-threshold harmonic generation. We also show that the short trajectory does not give rise to low-energy returns when initiated by tunnel ionization. Only when electrons are released close to the core, in a process mimicking multiphoton ionization, do we find a trajectory analogous to the short trajectory. This is true even for harmonics as high as the 27th, driven by a 1-μm laser in hydrogen.

Our article is organized as follows: In Sec. II we show fully quantum mechanical calculations of the quantum path contributions to harmonics 7–13 of a 1.07-μm laser in hydrogen, providing a benchmark for comparisons with results of our generalized SCM. Section III presents our generalized theory and how the different initial conditions are implemented. In Sec. IV we show results and compare the semiclassical calculations to the fully quantum result, and in Sec. V we briefly summarize our results and conclusions. All calculations are in atomic units with $\hbar = m_e = e = 1$ unless otherwise specified.

II. QUANTUM PATH DISTRIBUTIONS FOR LOW-ORDER HARMONICS

The process of harmonic generation results from the creation of a time-dependent dipole moment that has Fourier

components at frequencies $q\omega$, where q is an odd integer and ω is the driving laser frequency. In the SCM of high harmonic generation [7,17] the dipole moment at the qth harmonic d_q is first written as a sum over a small number of contributions, each characterized by a phase S_q^j:

$$d_q(I) \sim \sum_j a_j \, e^{iS_q^j}. \tag{1}$$

The different contributions are called quantum orbits. In the simplest approximation the real part of the phase S_q^j can be calculated from the action along the jth classical trajectory that returns an electron, freed by tunnel ionization, to the nucleus with kinetic energy T_r such that $E_{\rm ph} = T_r + I_p$. In the standard SCM the effect of the atomic potential on the electron trajectory is ignored and the classical action scales with the laser intensity as

$$S_q^j = -\alpha_j U_p/\omega, \tag{2}$$

where $U_p = I/4\omega^2$ is the ponderomotive energy and I is the laser intensity, both in atomic units. The phase coefficient α_j characterizes the quantum orbit and depends only on the return time (and not the intensity) when the effects of the potential are ignored. The different trajectories then have a dipole phase proportional to αI [5,6]. In the standard SCM, α varies between 0 and 2π for electron trajectories which return within one cycle of their ionization.

To make the connection between full quantum mechanical calculations and this semiclassical picture, we begin by writing the full intensity-dependent dipole moment $d_q(I)$ as the sum of contributions characterized by a parameter α that is conjugate to the intensity [18,19]:

$$d_q(I) = \int \tilde{d}_q(\alpha) e^{-i\alpha U_p(I)/\omega} d\alpha. \tag{3}$$

We then attempt to extract the dominant phase contributions to d_q from a full quantum mechanical calculation and compare them with the semiclassical phases α_j. We do this by calculating the complex intensity-dependent d_q via numerical integration of the time-dependent Schrödinger equation (TDSE) in two dimensions [20] for a hydrogen atom interacting with an intense, linearly polarized 1.07-μm laser pulse with a quasiconstant peak intensity. Starting from the ground-state wave function of the hydrogen atom calculated on our numerical grid, we numerically integrate the TDSE forward in time for the duration of the laser pulse. We do this for many different intensities. We calculate the dipole spectrum for each intensity from the time-dependent acceleration of the electron, $\langle a(t)\rangle = -\langle\psi(t)|[H,[H,z]]|\psi(t)\rangle$, where $\psi(t)$ is the time-dependent wave function and H is the Hamiltonian which includes both the laser and atomic potentials. The frequency-dependent dipole moment is then calculated from the Fourier transform of $a(t)$: $\tilde{d}(\omega) = -\tilde{a}(\omega)/\omega^2$.

For each harmonic q, and each intensity I_0, we then analyze the intensity-dependent dipole moment $d_q(I_0)$ in terms of the conjugate phase variable α, as described in [18]:

$$\tilde{d}_q(\alpha, I_0) = \int d_q(I) e^{i\alpha U_p(I)/\omega} W(I - I_0) dI, \tag{4}$$

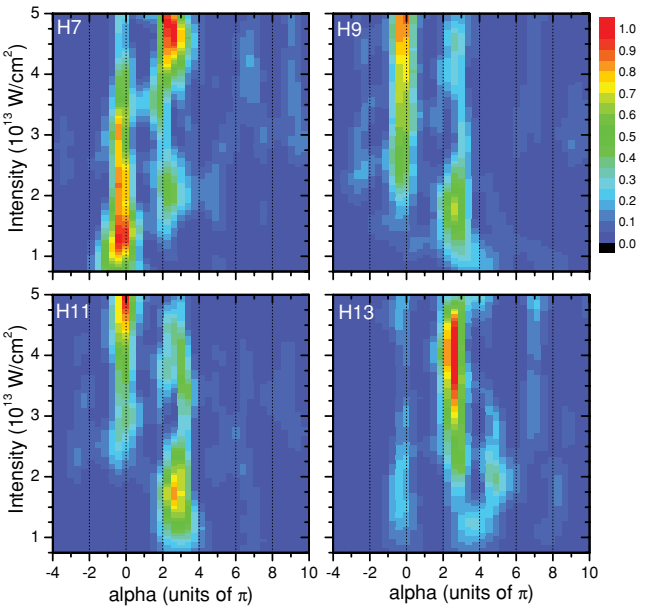

FIG. 1. (Color online) Quantum path distributions for harmonics 7 through 13 of a 1.07-μm laser in hydrogen. The mostly vertical (colored) strips indicate α values of the dominant contributions to the dipole phase.

where $W(I - I_0)$ is the same window function centered on I_0 used in [18], and $\tilde{d}_q(\alpha, I_0)$ represents the strength of the contribution to the intensity-dependent dipole moment which has a phase proportional to αI. For above-threshold harmonics, the phase coefficients obtained in this way from the full quantum calculations correspond well to those predicted by the SCM [18]. In particular, the short and long trajectories give rise to phase coefficients $\alpha_1 \approx 0.1\pi$–0.2π and $\alpha_2 \approx 2\pi$, respectively.

In this article we extend this analysis to harmonics below and close to threshold [1]. We begin by showing the result of the quantum path analysis for harmonics 7–13 of a 1.07-μm laser in hydrogen in Fig. 1. At this laser wavelength harmonic 13 is just above threshold. Each harmonic exhibits multiple quantum path contributions; the two dominant ones have phase coefficients $\alpha_0 \approx 0$ and $\alpha_2 \approx 2.5\pi$–3π. This α_2 is slightly larger than that predicted by the standard SCM for above-threshold harmonics. However, previous studies have found that quantum paths somewhat longer than the long trajectories (returning after more than one laser cycle) also dominate for higher harmonics [19]. We also note that the value of α_0 is actually slightly negative for all of these harmonics, which is very different from the predictions of the standard SCM, where α is always positive. Harmonics 3 and 5 exhibit only this α_0 contribution.

In the rest of this article we argue that the large α_2 contributions in Fig. 1 can be interpreted as generalized long trajectories which are relatively insensitive to the atomic potential except at low intensities. We also argue that there are no short trajectories initiated by tunnel ionization which lead to below-threshold return energies. We show that the $\alpha_0 \approx 0$ contribution can be reproduced if electrons are released at the ion core with a small kinetic energy.

III. GENERALIZED SEMICLASSICAL MODEL

In the simplest SCM for the phase coefficients α_j, an electron tunnel ionizes at time t_0 and is released into the laser field at the position of the ion core [$x(t_0) = 0$] with zero kinetic energy [$p(t_0) = 0$]. After the initial tunneling, the electron is considered to be solely under the influence of the laser, with potential energy $U(x,t) = \mathcal{E}(t)x$, where $\mathcal{E}(t)$ is the time-dependent laser electric field. Only electrons which return to the core at time t_r [$x(t_r) = 0$] will emit harmonics via recombination [2–4]. The phase accumulated by the electron wave function along a returning trajectory is given by the integral of the Lagrangian between the times of release and return [4]:

$$S(t_0,t_r) = \int_{t_0}^{t_r} (T - U)\, dt = \int_{t_0}^{t_r} -\frac{[p(t)]^2}{2}\, dt. \tag{5}$$

The last equality follows from Newton's equation and the initial and final conditions of the trajectory. The kinetic energy can be expressed in units of the ponderomotive energy, and we again define the phase coefficient α by $S = -\alpha\, U_p/\omega$, which is consistent with the form of the intensity-dependent phase we used in Eq. (3). With this convention α has units of radians and is always greater than or equal to zero. The short trajectory has a lower α than the long trajectory because it interacts with the laser for smaller periods of time.

In the generalized model we include the atomic potential explicitly. We use a soft-core potential,

$$U_a(x) = -\frac{1}{\sqrt{x^2 + \left(\frac{1}{U_0}\right)^2}}, \tag{6}$$

with a depth $U_0 = 0.707$ a.u. (19.2 eV) and a ground-state energy of -13.6 eV in order to approximate a hydrogen atom. The combined potential now becomes, in atomic units,

$$U(x,t) = \mathcal{E}(t)x + U_a(x), \tag{7}$$

where $\mathcal{E}(t) = \mathcal{E}_0 \sin(\omega t)$. Using the force derived from this potential, we integrate Newton's equation to obtain the trajectory for an electron released at a time t_0 during the laser cycle. The initial conditions $x(t_0)$ and $p(t_0)$ are described in detail in what follows. We consider only trajectories that are released between 0 and 0.5 laser cycles and return within the first two cycles of their release time.

As we determine the dynamics for each specific release, we calculate the phase associated with the motion. The phase accumulated in the combined potential now has a term which depends explicitly on the proximity of the electron to the ion core, $U_a(x)$:

$$S(t_0,t_r) = \int_{t_0}^{t_r} \left(\frac{[p(t)]^2}{2} - \mathcal{E}(t)x(t) - U_a(x) \right) dt. \tag{8}$$

To simplify this, we use $\dot{p} = -\mathcal{E}(t) - \partial U_a/\partial x$ and integrate the resulting $\dot{p}x$ by parts (remembering that $px|_{t_0}^{t_r} = 0$ in our generalized conditions). This yields the following expression for the action

$$\begin{aligned} S(t_0,t_r) &= \int_{t_0}^{t_r} \left(-\frac{[p(t)]^2}{2} + x(t)\frac{\partial}{\partial x}U_a(x) - U_a(x) \right) dt \\ &= \int_{t_0}^{t_r} \left(-\frac{[p(t)]^2}{2} + \Delta V \right) dt, \end{aligned} \tag{9}$$

where ΔV is given by

$$\Delta V = x(t)\frac{\partial}{\partial x}U_a(x) - U_a(x) = \frac{2x^2 + 1/U_0^2}{\left[x(t)^2 + \left(\frac{1}{U_0}\right)^2\right]^{3/2}}. \tag{10}$$

The presence of the atomic potential changes the phase both directly, through the ΔV contribution, and indirectly via its influence on the trajectories, which will be reflected in the $-p^2/2$ contribution. It is clear from Eq. (9) that the phase in the generalized model is no longer simply proportional to the laser intensity, for a given return energy. However, it is still useful to think about the harmonic phase as piecewise proportional to the laser intensity, especially for estimating the spatiotemporal coherence properties of the harmonic radiation [8,9]. We calculate such a generalized phase coefficient in two different ways. Conceptually, the simplest approach is to do a Taylor expansion of the phase in powers of the ponderomotive energy and thereby define the phase coefficient for a given harmonic q at a given intensity I as

$$\alpha_q(I) = -\frac{\partial}{\partial U_p}[\omega S_{|t_{\rm ret}}], \tag{11}$$

where the subscript on the phase means that we evaluate the derivative at a fixed return time [21]. This expression is numerically cumbersome to evaluate because it requires keeping track of and interpolating between at least two different sets of trajectories for many different intensities. In most of the calculations shown in this article, we have therefore calculated the intensity-dependent phase coefficients by using Eq. (4). We first calculate the intensity-dependent phase from the first four returning trajectories leading to some harmonic energy $q\omega$. Then we construct an intensity-dependent "dipole moment" by adding the complex phase terms according to Eq. (1), using equal and constant values $a_j = 1$. Finally we calculate the semiclassical path distribution of the constructed dipole moment using the same analysis [Eq. (4)] as we did for the fully quantum mechanical dipole moment. We note that in the quantum path analysis of the quantum dipole moment we also use a constant amplitude $|d_q(I)| = 1$ for the dipole moment as a function of intensity and retain only the phase information. This is sufficient information for performing the quantum path analysis; we refer to [18] for details.

A. Initial conditions

When the atomic potential is present, an electron at $x(t_0) = 0$ with $p(t_0) = 0$ will be bound and unable to escape from the influence of the atom. We have considered two types of initial conditions for the electron in the generalized model (Fig. 2) [22].

The initial conditions closest to that of the standard SCM are given by releasing the electron via tunneling through the potential barrier formed by the combined laser and atomic potential, with $x(t_0) \neq 0$ and $p(t_0) = 0$. We estimate $x(t_0)$ using a simplified Coulomb potential $U_a(x) = -1/x$ and finding where the combined potential equals the ionization potential outside of the barrier, which yields

$$x(t_0) = \frac{I_p + \sqrt{I_p^2 - 4|\mathcal{E}(t_0)|}}{2|\mathcal{E}(t_0)|}. \tag{12}$$

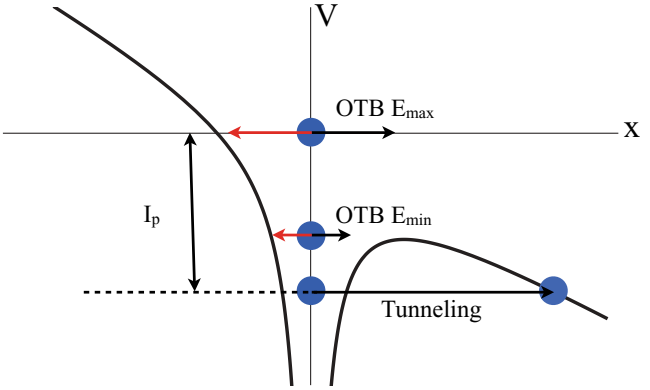

FIG. 2. (Color online) Visual representation of the initial conditions with atomic potential included. The red and black arrows represent the uphill and downhill OTB trajectories, respectively.

In the Results section, we refer to these trajectories as tunneling trajectories. To prevent extremely unlikely (large) tunneling distances, we have filtered out all results with initial positions greater than 25 a.u.

Another approach that can lead to below-threshold harmonics is to allow the electron a classical over-the-barrier (OTB) escape. Here we assume that the electron has been excited to some energy E_i while at $x = 0$, similar to multiphoton ionization. In other words, we create the initial conditions

$$x(t_0) = 0; \quad p(t_0) = \pm\sqrt{2(E_i + U_0)}. \tag{13}$$

This gives rise to two possible classes of trajectories for the electron. The first occurs when the electron initially moves downhill with respect to the potential. The electron spends its energy going over the potential bump caused by the distortion in the atomic potential by the laser. It is then mostly free from the atomic potential and has an extra"kick" behind it which influences whether it returns and, if it does, with how much energy.

The second class of trajectories occurs when the electron initially moves uphill with respect to the potential wall caused by the addition of the atomic and laser potentials. These trajectories return almost immediately to $x = 0$ and then continue to follow a trajectory similar to that of the first class.

There are two reasonable energy limits for the OTB initial conditions. Our upper limit is $E_i = 0$, which gives the electron enough energy to escape the atom in the absence of the laser potential. Our lower limit is $E_i = E_{\min} = -2\sqrt{|\mathcal{E}(t_0)|}$, or the maximum height of the barrier at the time of release. Since the electron has a finite velocity and the height of the barrier is constantly changing, the electron will have either an excess or deficiency of energy when encountering the barrier. On a deficiency, the electron returns quickly. We allow the electron to be released with any energy between these two limits and thus consider a range of different trajectories within this type of initial condition.

IV. RESULTS

Figure 3(a) shows the travel time as a function of return energy for an intensity of 10^{14} W/cm^2, for trajectories which return within (approximately) one cycle of their release. We

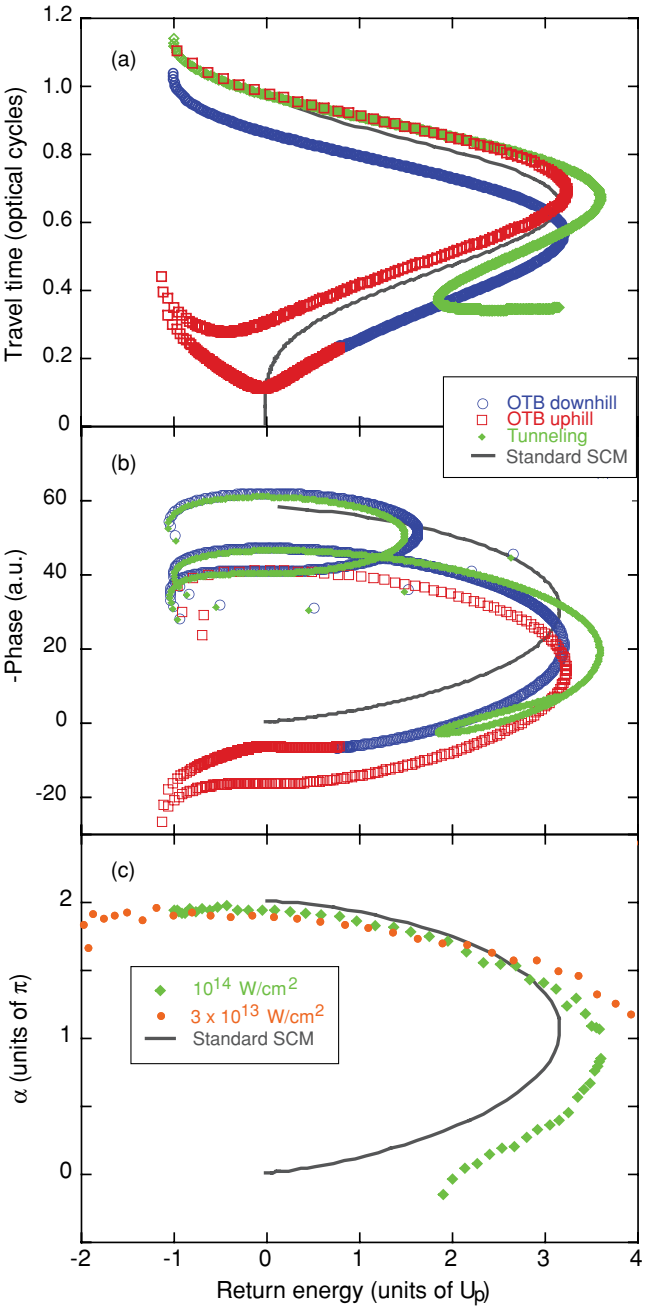

FIG. 3. (Color online) (a) Travel time versus return energy and (b) phase versus return energy, both for an intensity of 10^{14} W/cm^2. Results from the tunneling trajectories are shown with (green) diamonds. Results from the OTB trajectories are shown with (red) squares for uphill trajectories and (blue) circles for downhill trajectories. With the thin solid line we show the result of the standard SCM. (c) Phase coefficient versus return energy calculated within the tunneling model, using Eq. (11), for intensities of 10^{14} W/cm^2 (green diamonds) and 0.3×10^{14} W/cm^2 (orange circles).

show results both from the tunneling model and from the OTB model. For the latter we have chosen $E_i = 0$ in Eq. (13). For reference, we also show the result of the standard SCM.

The figure demonstrates several interesting properties of the short and long trajectories for both sets of initial conditions. The long trajectory (upper branch of each curve) is clearly

recognizable and gives rise to below-threshold returns for both tunneling and OTB trajectories, with travel times in good agreement with the standard SCM. The short trajectory, however, depends strongly on the choice of initial conditions. In particular, in the tunneling model and the OTB downhill model the short trajectory does not lead to low-energy returns, even at relatively high intensity. Low-energy returns are only achieved by the OTB uphill trajectories, either upon their first return (travel times around 0.2 cycles) or upon their second return (travel times around 0.3–0.4 cycles). All three sets of initial conditions converge toward the standard SCM results at higher intensities or when using shallower potentials (not shown in the figure). In what follows we discuss in more detail the dynamics of specific trajectories in the different models in order to clarify the results shown in Fig. 3.

In Fig. 3(b) we show the accumulated phase along each of the trajectories shown in (a), calculated according to Eq. (9). The phases of the tunneling and OTB downhill trajectories are in general very similar for the longer trajectories, except in the cutoff region. In all three models, the large phase of the long trajectories and the small phase of the short trajectories can be recognized, in agreement with the standard SCM. Their total phase is overall reduced compared to the standard SCM because of the ΔV term in Eq. (9), which has the opposite sign of the $-p^2/2$ contribution. The second group of trajectories with low energy returns, with phases around 60 a.u. (upper branch) and slightly below 40 a.u. (lower branch), are second returns of trajectories very similar to the long trajectory, where the second return occurs after a very brief excursion into the continuum.

Figure 3(c) shows the phase coefficient α calculated within the tunneling model using Eq. (11) for two different peak intensities. Here we are only showing trajectories which return within the first cycle. The long trajectory behaves very similarly to the long trajectory in the standard SCM, whereas the short trajectory as mentioned earlier only exists for high return energies and generally gives smaller values of α than in the standard SCM. We note that the second-return trajectories shown in (b) in general give rise to phase coefficients which are very close to those of the long trajectory but are slightly larger than 2π.

The electron dynamics leading to long-trajectory below-threshold return energies in the tunneling model are illustrated in Fig. 4. In panel (a) we show the trajectory and in panel (b) we show the evolution of the kinetic and potential energy (from the electron-ion interaction) with time. In the standard SCM the electron along this trajectory would barely miss recombination because it would be returning with insufficient energy at a time when the laser field is against its motion. In our case, the atomic potential overcomes the field and pulls the electron (slowly, due to the opposing field) into the atom. This is easily seen in the returns in Fig. 4(b), indicated by maxima in the kinetic energy and minima in potential energy. We note that we have not included the potential energy from the electron-laser interaction, which is zero upon recombination. In the OTB model (not shown in Fig. 4), downhill trajectories are released into the continuum (at $x_0 = 0$) already traveling away from the core and behave very similarly to the tunneling trajectories, in that they can lead to long-trajectory, below-threshold returns.

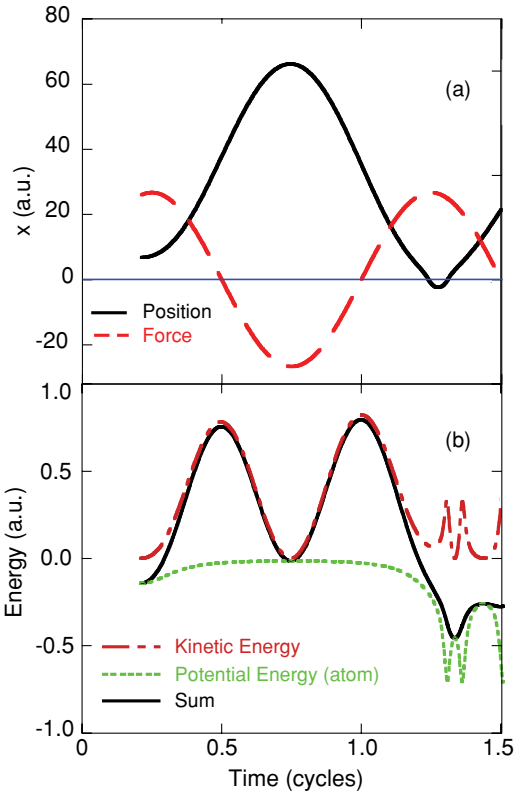

FIG. 4. (Color online) Long trajectory dynamics in the tunneling-initiated generalized SCM. (a) Position versus time. The dashed (red) line represents the force from the laser field. (b) Energy versus time of the identical trajectory. The intensity is 10^{14} W/cm^2 and the return energy is -0.25 a.u., which corresponds to $-0.58\ U_p$, or approximately the seventh harmonic.

The absence of low-energy returns for the short trajectory initiated by tunneling in the generalized SCM is illustrated in Fig. 5. The solid line shows a standard SCM low-energy short trajectory, which is released when the laser field is weak and spends only a very short time away from the core before returning with low energy. In our generalized SCM (dashed

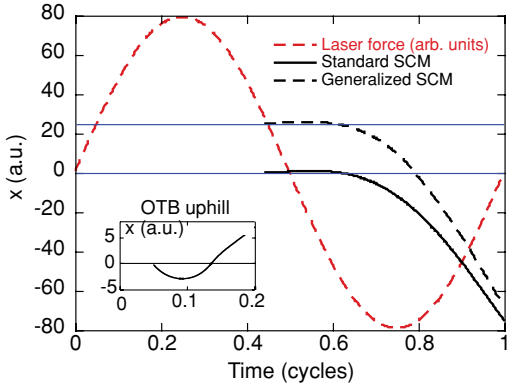

FIG. 5. (Color online) Dynamics of the short trajectory initiated by tunneling in the standard (solid black line) or generalized (dashed black line) SCM. The red dashed line represents the force from the laser field. (Inset) Position vs time for an uphill OTB trajectory, at an intensity of 10^{14} W/cm^2 and a return energy of -0.2 a.u., or close to the energy of harmonic 7.

line) the electron must tunnel very far when the laser field is weak and therefore must travel a long way to return back to the ion core, during which it is accelerated by the laser field (and by the attractive atomic potential) and returns with high energy. Thus, one difference between the short and long trajectories when including the atomic potential is whether the electron is being accelerated by the laser as it recombines (short trajectory) or slowed (long trajectory).

The electrons initially moving uphill in the OTB model can follow qualitatively different trajectories. In particular, such initial conditions allow for very short trajectories with below-threshold return energies in which the electron simply scatters off the potential and immediately returns. After this first return, some of the electrons can be reaccelerated on the other side and follow trajectories similar to the short and long trajectories, both of which exhibit low return energies. Both of the these uphill-initiated short trajectories can give rise to phase coefficients $\alpha \approx 0$ as we will show below. There are even a few downhill OTB trajectories which can lead to below-threshold return energies when we allow the initial energy of release to be low (between 0 and E_{min}). These electrons can be pulled back to the core by the atomic potential if they are released in a very weak field.

To compare to the quantum path calculations shown in Fig. 1, we have numerically solved the equations of motion for each model and release time at many different intensities. For the first four trajectories that return with a total energy corresponding to a particular harmonic energy $q\omega$, we calculate their phase S_q according to Eq. (9). We then construct an intensity-dependent dipole moment by summing all the different contributions as in Eq. (1) and calculate its "semiclassical path" distribution according to Eq. (4) [23]. Since we know the intensity-dependent phase of the individual trajectories, we also have the possibility to look at the distribution for the individual trajectories, which is then a measure of the intensity-dependent phase coefficients for that set of trajectories.

In Fig. 6 we show the total semiclassical path distribution of harmonics 7–13 generated in our tunneling model. By comparing to the quantum path calculations in Fig. 1, we see that the tunneling results match the longer quantum path contributions well, both in terms of the predicted values for α (around 2π) and in the (slight) increase of the phase coefficient as the intensity decreases. The figure also makes it clear (again) that there are no tunneling-initiated short trajectories for these low-order harmonics; that is, there are no trajectories that give rise to the small α contributions in Fig. 6. This is true for harmonics even substantially above threshold: the lowest harmonic that would exhibit a small-α contribution in a plot similar to Fig. 6 is harmonic 29. The four individual trajectories that are included in these harmonics have surprisingly similar phase coefficients (not shown in the figure). Some are slightly below 2π—among them the long trajectory, in agreement with Fig. 3(b)—and some are slightly above 2π, which makes the total semiclassical path distribution look like one strong contribution at 2π. Comparing to the quantum path distributions in Fig. 1 then suggests that the low-order harmonics have stronger contributions from the second return trajectories than from the long trajectory.

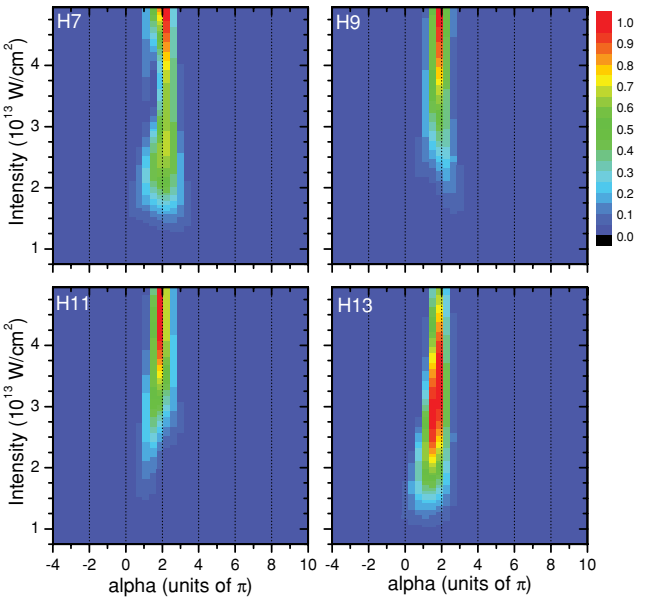

FIG. 6. (Color online) Semiclassical path distributions calculated from the generalized SCM, initiated by tunneling.

In Figs. 7 and 8 we show the semiclassical path distributions of the OTB downhill and uphill trajectories, respectively. For both figures we have chosen the initial energy to be $E_i = 0$, but the results for $E_i = E_{\text{min}}$ look very similar. The downhill results are in very good agreement with the tunneling results as discussed in connection with Fig. 3. The uphill results also reproduce the $\alpha \approx 0$ contribution in the quantum path distributions, even to the point of being slightly more negative than positive for harmonics 7 and 9 at the lowest intensities. Interestingly, the OTB uphill model is also the only model to exhibit a longer-trajectory phase coefficient which is larger than 2π, in agreement with both the experimental

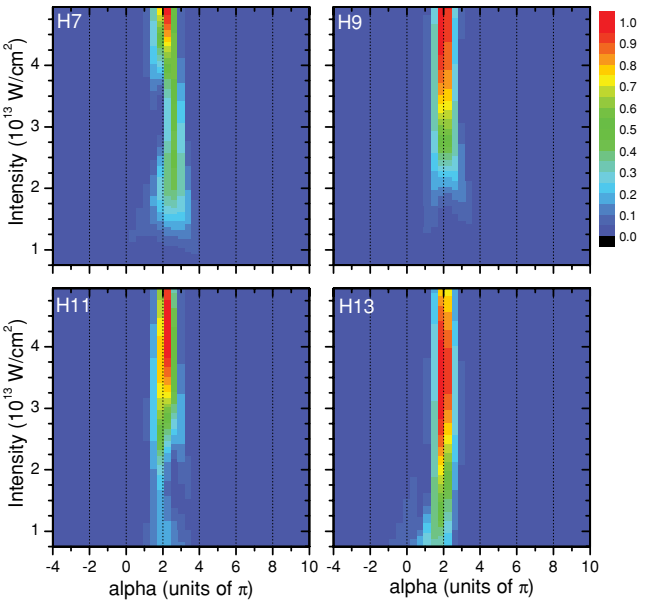

FIG. 7. (Color online) Semiclassical path distributions calculated from the generalized SCM, using the OTB model with downhill trajectories only.

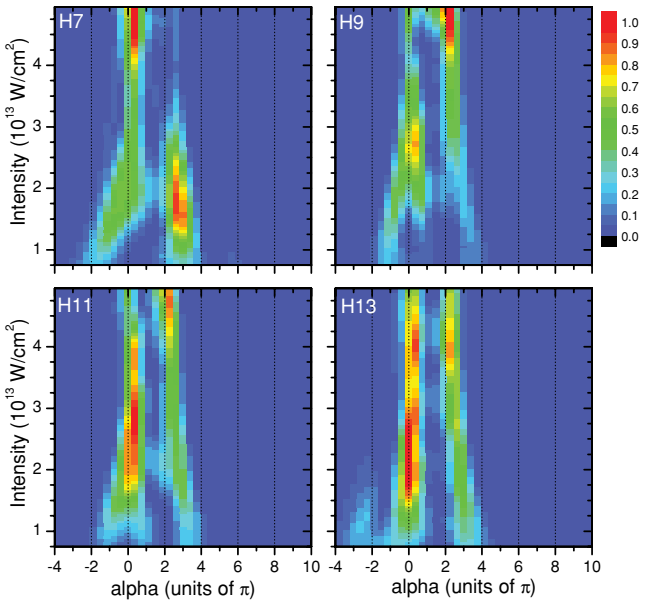

FIG. 8. (Color online) Semiclassical path distributions calculated from the generalized SCM, using the OTB model with uphill trajectories only.

measurement in [1] and the quantum mechanical calculations in Fig. 1. In the OTB uphill model, these values of α are due to both the long trajectory [with a travel time around 1 cycle in Fig. 3(a)] and trajectories with even longer travel times. Since we have restricted our classical calculations to trajectories which return to the core once or twice, our semiclassical path distributions do not exhibit any phase coefficients larger than approximately 4π.

For harmonics with energies above the ionization threshold, starting with harmonic 15, the tunneling and OTB downhill predictions for α are in good agreement with the long-trajectory component of the standard SCM: They exhibit the characteristic $\alpha_{\text{cutoff}} \approx \pi$ in the cutoff region, and this α slowly increases with intensity toward 2π. The OTB uphill prediction for the behavior of the short trajectory as a function of return energy is also in good agreement with the standard SCM [see Figs. 3(a) and 3(b)]. Our results are thus still in agreement with experimental measurements such as those in Refs. [9,24,25], in which the phase of the short-trajectory contribution to the harmonic emission (and thereby the emission time) has been found to increase with harmonic order, giving rise to a positive attochirp. In our generalized model the release mechanism for these short trajectories is different from that in tunneling, but the dynamics after release are very similar and still lead to larger accumulated phases for electrons that return later with higher energies.

V. SUMMARY

We have presented one approach to generalizing the semiclassical three-step model of harmonic generation, in which we have included the effects of the atomic potential in both the continuum dynamics of the electron and the initial ionization process. For the continuum dynamics, we included the atomic potential simply by solving the classical equations of motion for an electron moving in the combined laser-atomic potentials. For the ionization process we included the atomic potential via the choice of initial conditions, which we chose to mimic either (i) tunnel ionization, by releasing the electron outside the laser-induced potential barrier with zero velocity, or (ii) multiphoton ionization, by releasing the electron at the ion core with nonzero kinetic energy, moving either uphill or downhill with respect to the laser potential.

We calculated the intensity-dependent phase accumulated along the generalized semiclassical trajectories and found results in good agreement with a range of experimental measurements, as well as with fully quantum mechanical calculations in hydrogen. In particular, we found that there are semiclassical trajectories leading to return energies that are below the ionization threshold of our model atom, in agreement with the experimental observation of semiclassical dynamics in below-threshold harmonics in xenon [1], cesium [26], and the molecular gases N_2 and O_2 [27]. We showed that the long trajectory readily generalizes and is relatively insensitive to the choice of initial conditions. We also showed that there are no low-energy short trajectories initiated by tunneling in the generalized model, simply because tunneling releases the electron far from the core and it is subsequently accelerated all the way back by both the laser and the atomic potential. In contrast, the low-energy electrons returning along the long trajectory move against the laser field when they are close to the core, and can end up with below-threshold energies because they get "pulled in" by the attractive atomic potential. We note that a recent experimental study by Power *et al.* found that below-threshold harmonics in cesium exhibited semiclassical characteristics dominated by the long trajectory [26]. Finally, we showed that the short-trajectory characteristics well known from the standard SCM can be reproduced only if the electron is released into the continuum in a process which is closer to multiphoton than to tunnel ionization. Interestingly, in parallel with the writing of this article, experimental and theoretical studies by Soifer *et al.* show very similar results to what we are reporting here in terms of the contributions of both tunnel-ionized long trajectories and multiphoton-ionized short trajectories to the production of low-order harmonics [27].

The standard SCM has been very successful in its description of high-order harmonic generation. Our work presented here, along with a number of other studies [14–16,26,27], indicates that a generalized SCM may also be applied to the understanding of rescattering processes with energies much closer to the ionization potential. An expanded SCM represents a rich system for further study, since the choice of atomic potential, the choice of initial conditions, and the intensity all affect the trajectories and their phase behavior. In particular, we have found that the short trajectories, which spend most of their time close to the ion core, are sensitive to these choices and that there can be different classes of short trajectories, especially at low intensity.

ACKNOWLEDGMENTS

Funding at LSU was provided by the NSF through Grants No. PHY-0449235 (J.A.H. and J.L.T.) and No. PHY-0701372 (K.J.S.). K.J.S. acknowledges support from the Ball Family Professorship. M.B.G. acknowledges support from the PULSE Institute at Stanford University.

[1] D. C. Yost, T. R. Schibli, J. Ye, J. L. Tate, J. Hostetter, M. B. Gaarde, and K. J. Schafer, Nat. Phys. **5**, 815 (2009).
[2] K. J. Schafer, B. Yang, L. F. DiMauro, and K. C. Kulander, Phys. Rev. Lett. **70**, 1599 (1993).
[3] P. B. Corkum, Phys. Rev. Lett. **71**, 1994 (1993).
[4] M. Lewenstein, Ph. Balcou, M. Yu. Ivanov, A. L'Huillier, and P. B. Corkum, Phys. Rev. A **49**, 2117 (1994).
[5] M. Lewenstein, P. Salières, and A. L'Huillier, Phys. Rev. A **52**, 4747 (1995).
[6] P. Antoine, A. L'Huillier, and M. Lewenstein, Phys. Rev. Lett. **77**, 1234 (1996).
[7] P. Salières *et al.*, Science **292**, 902 (2001).
[8] M. Bellini, C. Lyngå, A. Tozzi, M. B. Gaarde, T. W. Hänsch, A. L'Huillier, and C.-G. Wahlström, Phys. Rev. Lett. **81**, 297 (1998).
[9] Y. Mairesse *et al.*, Science **302**, 1540 (2003).
[10] P. Balcou, P. Salières, A. L'Huillier, and M. Lewenstein, Phys. Rev. A **55**, 3204 (1997).
[11] S. Kazamias and Ph. Balcou, Phys. Rev. A **69**, 063416 (2004).
[12] W. Becker, A. Lohr, S. Long, J. K. McIver, B. N. Chichkov, and B. Wellegehausen, Laser Physics **7**, 88 (1997).
[13] A. Zaïr *et al.*, Phys. Rev. Lett. **100**, 143902 (2008).
[14] P. J. Ho and J. H. Eberly, Opt. Express **11**, 2826 (2003).
[15] T. Nubbemeyer, K. Gorling, A. Saenz, U. Eichmann, and W. Sandner, Phys. Rev. Lett. **101**, 233001 (2008).
[16] E. S. Shuman, R. R. Jones, and T. F. Gallagher, Phys. Rev. Lett. **101**, 263001 (2008).
[17] D. B. Milosevic, D. Bauer, and W. Becker, J. Mod. Opt. **53**, 125 (2006).
[18] Ph. Balcou, A. S. Dederichs, M. B. Gaarde, and A. L'Huillier, J. Phys. B **32**, 2973 (1999).
[19] M. B. Gaarde and K. J. Schafer, Phys. Rev. A **65**, 031406(R) (2002).
[20] K. J. Schafer and K. C. Kulander, Phys. Rev. Lett. **78**, 638 (1997).
[21] In the standard SCM, keeping the return time constant is equivalent to keeping the return energy constant when measured as a fraction of U_p.
[22] M. Y. Ivanov, M. Spanner, and O. Smirnova, J. Mod. Opt. **52**, 165 (2005).
[23] We have tried weighting the four different paths equally, or weighting the ones with longer return times slightly lower, to account for the dispersion that would occur for a quantum wave packet. This spread is proportional to the square root of the travel time. We find that the weighting makes little difference for the appearance of the semiclassical path distributions.
[24] N. Dudovich, O. Smirnova, J. Levesque, Y. Mairesse, M. Yu. Ivanov, D. M. Villeneuve, and P. B. Corkum, Nat. Phys. **2**, 781 (2006).
[25] J. M. Dahlstrom, T. Fordell, E. Mansten, T. Ruchon, M. Swoboda, K. Klunder, M. Gisselbrecht, A. L'Huillier, and J. Mauritsson, Phys. Rev. A **80**, 033836 (2009).
[26] E. P. Power, A. M. March, F. Catoire, E. Sistrunk, K. Krushelnick, P. Agostini, and L. F. DiMauro, Nat. Photonics **4**, 352 (2010).
[27] H. Soifer, P. Botheron, D. Shafir, A. Diner, O. Raz, B. Bruner, Y. Mairesse, B. Pons, and N. Dudovich (unpublished).